Dependence on crossing angle of electron beam slicing in storage rings

A. He, F. Willeke, and L. H. Yu

Photon Sciences Division, Brookhaven National Laboratory, Upton, New York 11973, USA

(Received 3 June 2014; published 17 December 2014)

When a low energy electron bunch (~20 MeV) crosses from top of a high energy bunch (e.g., 3 GeV) at an angle (e.g., 45°), the Coulomb force exerted on the high energy bunch by the low energy bunch will kick a very short (~150 fs) slice from the core of the high energy bunch. The slice of electron bunch can generate ultrashort x-ray pulse. In this paper, we will give analytical expressions about the angular kicks dependence on the crossing angle by assuming a Gaussian distribution for the low energy bunch. Applying the analytical results to the storage ring bunch in NSLS-II [1], we will discuss the optimized parameters of the electron beam slicing system in order to obtain a very short slice bunch and a sufficient separation between the slice and the core bunch.

DOI: 10.1103/PhysRevSTAB.17.120704 PACS numbers: 52.59.Px

I. INTRODUCTION

With the rapid increase in the requirements for sub-pic-second x-ray pulses in science, several approaches to generate ultrashort x-ray pulses have been proposed. Each of them has their own characteristics, for example, the pulse duration from laser slicing [2–7] can reach the order of 100 fs, the pic-second x-ray pulses generated by the crab cavity method [8–10] have high average flux ($\sim 10^{14}$ photons/ sec /0.1%bw) and high repetition rate (several hundreds MHz), the pulses produced from x-ray free electron laser [11] are good at higher pulse energy and shorter pulse width. The electron beam slicing method [12,13] is a new method to produce ultra-short x-ray pulse which has several features in space-saving, short pulse duration (~150 fs), high flux ($\sim 10^9$ photons/ sec / 0.1%bw), high repetition rate (100 kHz − 1 MHz) and stability etc. The electron beam slicing method, as illustrated in Fig. 1, uses a focused short low energy (~20 MeV) electron bunch to slice a short electron bunch from the electron bunches in a synchrotron radiation storage ring. When the low energy electron bunch crosses from top of the high energy electron bunch at right angle, its Coulomb force will kick a short slice of high energy electrons away from the core of the storage ring electron bunch. The separated slice when passing through an undulator will radiate ultrashort x-ray pulses at about 150 fs.

In this paper we derive the analytical expressions for the angular kicks dependence on the crossing angle induced by the Coulomb force during the crossing time of the two bunches. We discuss the parameter requirements of the electron beam slicing system, i.e., the low energy bunch beam size and the crossing angle, in order to carry out electron beam slicing experiment in the storage ring of NSLS-II. We organize this paper as follows: In Sec. II, we derive the vertical integrated angular kick as a function of the crossing angle and the 3-D position of the storage ring bunch which includes a profile function with three scaling parameters. In Sec. III, the main performances of the e-beam slicing method is illustrated through an example. The conditions of the maximum kick and the estimated slice bunch width are given. The influence of the low energy bunch's 3-D beam size and the crossing angle on the maximum kick angle are then discussed in depth. The dependence of the slice bunch width on the crossing angle is also considered. In Sec. IV, we discuss the horizontal kick and the longitudinal energy modulation. In Sec. V, the reaction of the high energy storage ring bunch on the low energy linac bunch is described. Concluding remarks are given in Sec. VI.

II. ANGULAR KICK θ_y

For simplicity, we label the high energy storage ring bunch as bunch 1 and the low energy linac bunch as bunch 2. We start from the Coulomb force exerted on the storage ring electron 1 by the low energy electron 2, then derive the vertical angular kick $\Delta\theta_y$ generated by a point charge in the low energy bunch 2. We assume the low energy bunch 2 has a Gaussian distribution in x, y, z direction respectively and obtain the angular kick θ_y generated by the whole bunch 2 through integrating $\Delta\theta_y$ over the 3-D electron beam distribution of bunch 2.

A. Force exerted on the high energy storage ring electron by the low energy linac electron

In Fig. 1, the high energy storage ring electron 1 moves in the xoz plane along the direction which has angle φ with

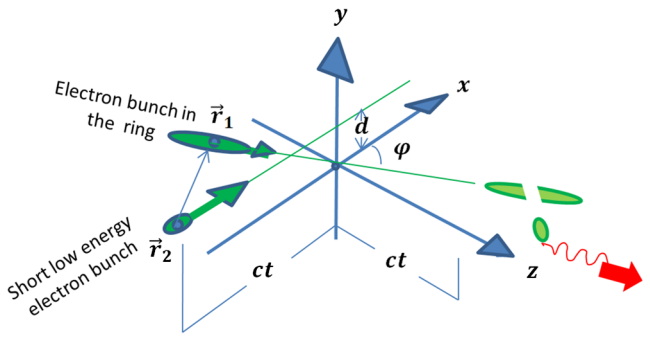

FIG. 1. Illustration of electron beam slicing.

axis "$+x$" with relative velocity β_1. The low energy linac electron 2 moves in the xoy plane along the "$+x$" direction with relative velocity β_2. The electric field at position $\vec{r}_1$ contributed by the electron 2 at position $\vec{r}_2$ can be expressed by [14]

$$\vec{E} = \frac{e}{4\pi\varepsilon_0}\frac{\gamma_2}{S^3}\vec{r}, \tag{1}$$

where ε_0 is the permittivity of free space, $S = \sqrt{\gamma_2^2 x^2 + y^2 + z^2}$, $\vec{r} = \vec{r}_1 - \vec{r}_2$. The corresponding magnetic field can be calculated by $c\vec{B} = \vec{\beta}_2 \times \vec{E}$. Then the force exerted on electron 1 by electron 2 is

$$\begin{aligned}\vec{F} &= e\vec{E} + e\vec{v}_1 \times \vec{B} \\ &= e(1 - \beta_1\beta_2\cos\varphi)\vec{E} + e\beta_1\beta_2(\cos\varphi E_x + \sin\varphi E_z)\vec{x},\end{aligned} \tag{2}$$

where we use $\hat{x} \times (\hat{x} \times \vec{E}) = E_x\hat{x} - \vec{E}$, $\hat{z} \times (\hat{x} \times \vec{E}) = E_z\vec{x}$.

We assume that when $t = 0$ electron 1 locates at position (x_1, y_1, z_1) and electron 2 locates at position $(x_2, y_2 + d, z_2)$, where d is the vertical distance between the high energy storage ring beam line and the low energy linac beam line. Because $v_{\vec{r}_1} \approx c$, $v_{\vec{r}_2} \approx c$, at time t, electron 1 moves to $(x_1 + ct\cos\varphi, y_1, z_1 + ct\sin\varphi)$ and electron 2 moves to $(x_2 + ct, y_2 + d, z_2)$. Inserting Eq. (1) into Eq. (2), the force can be rewritten as

$$\vec{F} = \frac{e^2}{4\pi\varepsilon_0}\frac{\gamma_2}{S^3}\begin{cases}[x + (\beta_1\beta_2\sin\varphi)z]\vec{x} \\ [(1 - \beta_1\beta_2\cos\varphi)y]\vec{y} \\ [(1 - \beta_1\beta_2\cos\varphi)z]\vec{z}\end{cases}. \tag{3}$$

Using the coordinates x_r, y_r, z_r of the storage ring bunch, the forces exerted on the storage ring electron by the linac electron in the horizontal, vertical and longitudinal direction are $F_{x_r} = (F_x\sin\varphi - F_z\cos\varphi)$, $F_{y_r} = F_y$, $F_{z_r} = (F_x\cos\varphi + F_z\sin\varphi)$, respectively. Therefore the force, expressed in terms of the coordinates of the storage ring bunch, is

$$\begin{pmatrix}F_{x_r} \\ F_{y_r} \\ F_{z_r}\end{pmatrix} = \frac{e^2}{4\pi\varepsilon_0}\frac{\gamma_2}{S^3}\begin{pmatrix}x\sin\varphi + z(\beta_1\beta_2 - \cos\varphi) \\ y(1 - \beta_1\beta_2\cos\varphi) \\ (x\cos\varphi + z\sin\varphi)\end{pmatrix}, \tag{4}$$

where $x = -(x_2 - x_1) - ct(1 - \cos\varphi)$, $y = -(y_2 - y_1) - d$, $z = -(z_2 - z_1) + ct\sin\varphi$. Notice the force components in the storage ring coordinate system is expressed in terms of the low energy bunch coordinates.

B. Angular kick $\Delta\theta_y$ by single low energy particle

We assume each low energy particle's point charge is q_2. According to Eq. (4), the kick force on electron 1 in the vertical direction $\vec{y}$ can be expressed as

$$F_y = -\frac{eq_2}{4\pi\varepsilon_0}\frac{\gamma_2}{S^3}(1 - \beta_1\beta_2\cos\varphi)(d + y_2 - y_1). \tag{5}$$

The relation between the kick force and the kick angle can be expressed as

$$F_y = \gamma_1 mc\frac{d\theta_y}{dt} = \frac{E_1}{c}\frac{d\theta_y}{dt}, \tag{6}$$

where we use $\frac{dy}{dt} \approx c\theta_y$ due to $v_{\vec{r}_1} \approx c$, E_1 is the energy of the storage ring electron 1. The angular kick $\Delta\theta_y$ generated by a point charge in the low energy bunch 2 can be obtained by integrating $d\theta_y = (cF_y/E_1)dt$ over the crossing time:

$$\begin{aligned}\Delta\theta_y &= \frac{eq_2\gamma_2 c}{4\pi\varepsilon_0 E_1}\int_{-\infty}^{+\infty}\frac{dt}{S^3}(1 - \beta_1\beta_2\cos\varphi)(d + y_2 - y_1) \\ &= \frac{eq_2 Z_0 c}{2\pi E_1}\cdot\frac{\gamma_2(1 - \beta_1\beta_2\cos\varphi)}{[\gamma_2^2(1 - \cos\varphi)^2 + \sin^2\varphi]^{1/2}}\cdot\frac{d + y_2 - y_1}{a^2},\end{aligned} \tag{7}$$

where $Z_0 = \frac{1}{\varepsilon_0 c} = 377\Omega$ and

$$\begin{aligned}a^2 = &\frac{\gamma_2^2}{\gamma_2^2(1 - \cos\varphi)^2 + \sin\varphi^2} \\ &\times [(x_2 - x_1)\sin\varphi + (z_2 - z_1)(1 - \cos\varphi)]^2 \\ &+ (d + y_2 - y_1)^2.\end{aligned}$$

In Eq. (7), we removed a minus sign for the $\Delta\theta_y$ which is due to the minus sign of Eq. (5). That means we define $\Delta\theta_y$ positive if the electron is kicked downward as shown in Fig. 1.

C. Angular kick θ_y by a Gaussian low energy bunch

We assume the low energy bunch 2 has a Gaussian distribution in x, y, z direction and the RMS bunch size is $\sigma_x, \sigma_y, \sigma_z$, respectively. Integrating $\Delta\theta_y$ over the whole low energy bunch 2, we obtain the angular kick generated by the low energy bunch on the storage ring electron as:

$$\theta_y = \frac{eq_2 Z_0 c}{2\pi E_1}\cdot\frac{\gamma_2(1-\beta_1\beta_2\cos\varphi)}{[\gamma_2^2(1-\cos\varphi)^2+\sin^2\varphi]^{1/2}}\cdot\frac{1}{(2\pi)^{3/2}\sigma_x\sigma_y\sigma_z}\cdot I_y, \tag{8}$$

where

$$I_y = \iiint_V e^{-\frac{x_2^2}{2\sigma_x^2}} e^{-\frac{y_2^2}{2\sigma_y^2}} e^{-\frac{z_2^2}{2\sigma_z^2}}\cdot\frac{d+y_2-y_1}{a^2}\,dx_2dy_2dz_2. \tag{9}$$

Using the variable transform $x_2=\sqrt{2}\sigma_x x$, $y_2=\sqrt{2}\sigma_y y$, $z_2=\sqrt{2}\sigma_z z$, and the following defined scaling parameters:

$$\rho \equiv \sqrt{\frac{\gamma_2^2}{\gamma_2^2(1-\cos\varphi)^2+\sin^2\varphi}\cdot\frac{\sigma_x^2\sin^2\varphi+\sigma_z^2(1-\cos\varphi)^2}{\sigma_y^2}}$$
$$\bar{y}_1 \equiv \frac{d-y_1}{\sqrt{2}\sigma_y}$$
$$\bar{u}_1 \equiv \frac{x_1\sin\varphi+z_1(1-\cos\varphi)}{\sqrt{2\sigma_x^2\sin^2\varphi+2\sigma_z^2(1-\cos\varphi)^2}}, \tag{10}$$

the triple integral of Eq. (9) can be reduced to the double integral:

$$I_y = 2\sqrt{\pi}\sigma_x\sigma_z\iint e^{-y^2-u^2}\frac{y+\bar{y}_1}{b^2}\,dydu, \tag{11}$$

where $b^2=(y+\bar{y}_1)^2+\rho^2(u-\bar{u}_1)^2$. Using the integral equation $\frac{\beta}{\pi}\int\frac{e^{-x^2}}{(x-\alpha)^2+\beta^2}dx=\mathrm{Re}[W(\alpha+i|\beta|)\mathrm{Sign}(\beta)]$ with $W(u)=e^{-u^2}\mathrm{erfc}(-iu)$ and error function $\mathrm{erfc}(x)=\frac{2}{\sqrt{\pi}}\int_x^{+\infty}e^{-x^2}dx$, Eq. (11) can be written as

$$I_y = 2\pi^{3/2}\sigma_x\sigma_z\int_0^\infty \mathrm{Re}[W(\bar{u}_1+iy)]\times[e^{-(\rho y-\bar{y}_1)^2}-e^{-(\rho y+\bar{y}_1)^2}]dy. \tag{12}$$

We now transform the storage ring particle's coordinates from the coordinate system defined relative to low energy bunch shown in Fig. 1 to the storage ring coordinate x_r, y_r, z_r by using the variable transform $x_1=z_r\cos\varphi+x_r\sin\varphi$, $y_1=y_r$, $z_1=z_r\sin\varphi-x_r\cos\varphi$, then $\bar{u}_1$ in Eq. (10) becomes $\bar{u}_1\equiv\frac{z_r\sin\varphi+x_r(1-\cos\varphi)}{\sqrt{2\sigma_x^2\sin^2\varphi+2\sigma_z^2(1-\cos\varphi)^2}}$. Inserting Eq. (12) into Eq. (8) and using the previous coordinates transform from x_1, y_1, z_1 to x_r, y_r, z_r, we obtain the final angular kick θ_y as:

$$\theta_y = \frac{eq_2Z_0c}{2\pi E_1}\frac{\gamma_2(1-\beta_1\beta_2\cos\varphi)}{\sqrt{\gamma_2^2(1-\cos\varphi)^2+\sin^2\varphi}}\frac{1}{\sqrt{2}\sigma_y}f_y(\rho,\bar{u}_1,\bar{y}_1), \tag{13}$$

where f_y gives the profile as a function of the high energy electron's position

$$f_y(\rho,\bar{u}_1,\bar{y}_1) = \int_0^\infty \mathrm{Re}[W(\bar{u}_1+iy)]\times[e^{-(\rho y-\bar{y}_1)^2}-e^{-(\rho y+\bar{y}_1)^2}]dy. \tag{14}$$

$\rho, \bar{u}_1, \bar{y}_1$ are given by

$$\rho \equiv \sqrt{\frac{\gamma_2^2}{\gamma_2^2(1-\cos\varphi)^2+\sin^2\varphi}\cdot\frac{\sigma_x^2\sin^2\varphi+\sigma_z^2(1-\cos\varphi)^2}{\sigma_y^2}}$$
$$\bar{y}_1 \equiv \frac{d-y_r}{\sqrt{2}\sigma_y}$$
$$\bar{u}_1 \equiv \frac{z_r\sin\varphi+x_r(1-\cos\varphi)}{\sqrt{2\sigma_x^2\sin^2\varphi+2\sigma_z^2(1-\cos\varphi)^2}}. \tag{15}$$

Equation (13) gives the angular kick as a function of the electron's 3-D position x_r, y_r, z_r in the storage ring bunch 1. The profile function Eq. (14) describes the profile of the slice bunch and can be used to estimate the pulse width of the slice.

III. NUMERICAL ANALYSIS

For this slicing method, we require that the vertical angular deviation of the slice bunch is large enough for the slice to be separated from the core bunch and the pulse length of the slice is small enough to radiate femtosecond x-ray. For the preliminary design, according to the kick function Eq. (13), we can determine the requirements on the low energy bunch performances, pick the interaction position in the storage ring of NSLS-II and choose the crossing angle between the two bunches.

The value of the kick angle in Eq. (13) can be separated into two parts: the nominal kick angle

$$\theta_{y0} = \frac{eq_2Z_0c}{2\pi E_1}\frac{\gamma_2(1-\beta_1\beta_2\cos\varphi)}{\sqrt{\gamma_2^2(1-\cos\varphi)^2+\sin^2\varphi}}\frac{1}{\sqrt{2}\sigma_y} \tag{16}$$

and the coefficient $f_y(\rho,\bar{u}_1,\bar{y}_1)$ which determines the profile of the slice bunch. Equation (16) shows that the nominal kick angle is proportional to the low energy bunch charge, inversely proportional to the storage ring energy E_1 and the vertical beam size σ_y of the low energy bunch. It also depends on the crossing angle φ, but is not sensitive to the low energy bunch energy γ_2 when it is much larger than one. From the cost point of view, we prefer the energy γ_2 of bunch 2 as low as possible. Therefore in our discussion, we choose $E_2=20$ MeV corresponding to $\gamma_2\approx 39$. The profile function $f_y(\rho,\bar{u}_1,\bar{y}_1)$ is basically a function of the particle position x_r, y_r, z_r of high energy electrons in the storage ring coordinate system and the crossing angle φ of the two bunches through the scaling function Eq. (15). The profile function gives the maximum angular kick condition and also describes the slice pulse width.

In the following analysis, we first give an example to explain what kind of performances of the e-beam slicing method we can expect. Then we will discuss how the low energy bunch size $\sigma_x, \sigma_y, \sigma_z$ and the crossing angle φ influence the maximum kick angle $\theta_{y,\max}$ and the slice width.

A. Numerical example

To estimate the possible range of the performances for the e-beam slicing experiment, we give a numerical example at NSLS-II [1] for the crossing angle $\varphi = 90°$. We assume the kick point is at a position in the storage ring where $\beta_x = 3.8$ m, $\beta_y = 25$ m, if the horizontal and vertical emittance is $\varepsilon_x = 1$ nm, $\varepsilon_y = 10$ pm, respectively, then the horizontal and vertical RMS beam divergence is $\sigma_x' = 16$ μrad, $\sigma_y' = 0.6$ μrad, respectively.

To separate the slice from the core bunch of the storage ring we estimate that the vertical angular kick should be more than 5 times larger than σ_y', i.e., $\theta_y > 3$ μrad. We assume the 20 MeV low energy electron bunch with charge of $q_2 = 200$ pC is focused to the horizontal and vertical beam size of $\sigma_z = \sigma_y = 35$ μm, and compressed to the longitudinal beam size $\sigma_x = 35$ μm, i.e., bunch length of about 120 fs. As an example, taking the storage ring energy as $E_1 = 3$ GeV, for crossing angle $\varphi = 90°$, we find the nominal kick angle as $\theta_{y0}(90°) = \frac{eq_2 Z_0 c}{2\pi E_1}\frac{\gamma_2}{\sqrt{\gamma_2^2+1}}\frac{1}{\sqrt{2}\sigma_y} = 24$ μrad. The profile parameter $\rho = \sqrt{\frac{\gamma_2^2}{\gamma_2^2+1}\cdot\frac{\sigma_x^2+\sigma_z^2}{\sigma_y^2}} = 1.4$. We choose the distance between the storage ring bunch's beam-line and the low energy bunch's beam-line as $d = \sqrt{2}\sigma_y = 50$ μm, which we find to give maximum kick. Assume $x_r = y_r = z_r = 0$, i.e., when the electron in the storage ring bunch arrives at the origin of the coordinate system, the center of the low energy bunch just arrives at the position on the top of the origin by vertical distance $d = 50$ μm, then we have $\bar{y}_1 = 1$, $\bar{u}_1 = 0$, and we find $f_y = 0.54$. The kick angle is given by $\theta_y(90°) = \theta_{y0}(90°) f_y = 13$ μrad, much larger than the required 3 μrad for the separation from the core.

The width of the slice is estimated by the width in $\bar{u}_1$ of the profile f_y at $\bar{y}_1 = 1$ and the horizontal beam size of the storage ring bunch adding in quadrature (we will discuss the slice width in more detail later in Sec. III D). For the above example $\sigma_x = \sigma_y = \sigma_z = 35$ μm, at the kick point with $\beta_x = 3.8$ m and $\varepsilon_x = 1$ nm, the horizontal FWHM of the storage ring bunch is about 145 μm and at $\rho = 1.4$ the FWHM of $\bar{u}_1$ is 2.5. Then the estimated FWHM of the slice bunch is about 227 μm which corresponds to 760 fs. As an estimate, we use an aperture to select x-rays from those electrons in the slice whose vertical angular divergence is larger than half of the maximum kick angle, then the peak to peak pulse width of the slice is 760 fs. Thus the estimated RMS value of slice width should be estimated roughly as one fourth of this peak to peak value, i.e., 190 fs. We can see the contribution of the horizontal crossing time dominates the pulse width. But, as we will discuss in more detail later in Sec. III D, we find that when the low energy bunch crosses the high energy bunch with an angle of 45° rather than 90°, this problem of horizontal crossing time can be overcome. Then, again, the width of $\bar{u}_1$ becomes important, and we can reach the slice length of the order of 107 fs.

B. Profile function f_y

To understand the relation of the angular kick and the scaling parameters, we plot the function f_y in Fig. 2 for the case of $\rho = 1.4$. The plot shows the maximum point locates at $\bar{u}_1 = 0, \bar{y}_1 = 1$. A set of plots of f_y as a function of $\bar{y}_1$ at $\bar{u}_1 = 0$ for different ρ are shown in Fig. 3. The maximum is always approximately at $\bar{y}_1 = 1$. That means if we choose the vertical distance between the two bunches center is $d = \sqrt{2}\sigma_y$, the electron in the storage ring bunch located at $x_r = 0, y_r = 0, z_r = 0$ will receive the maximum kick $\theta_{y,\max}$. The value of the maximum kick can be adjusted through the scaling parameter ρ by changing the crossing angle φ and the low energy bunch size $\sigma_x, \sigma_y, \sigma_z$. We also plot the profile of f_y as a function of $\bar{u}_1$ for $\bar{y}_1 = 1$ in Fig. 4 for different ρ. The width in $\bar{u}_1$ of the profile f_y at $\bar{y}_1 = 1$ can be used to estimate the width of the slice.

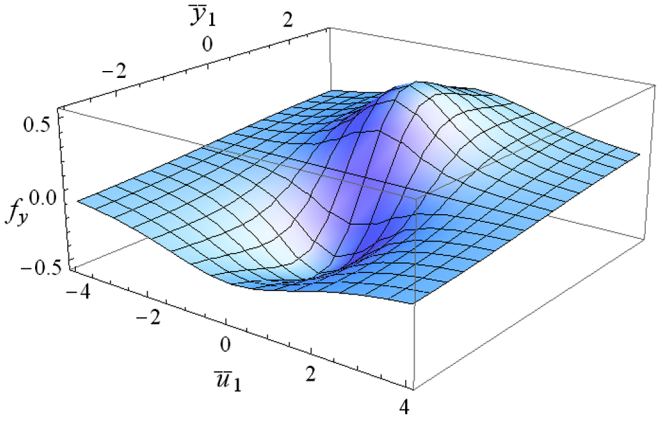

FIG. 2. Profile function f_y.

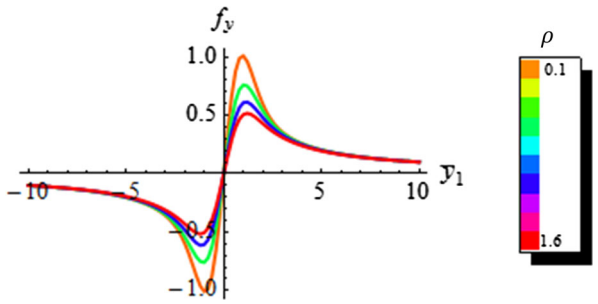

FIG. 3. Profile on axis $\bar{u}_1 = 0$. The maximum f_y locates at $\bar{y}_1 = 1$.

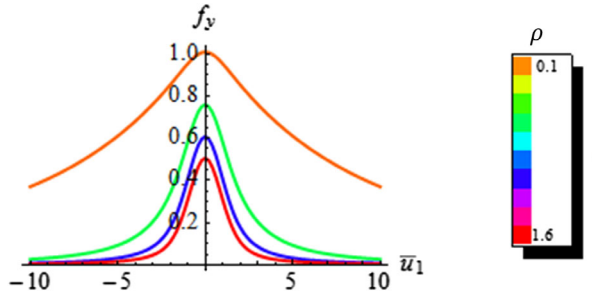

FIG. 4. Profile on axis $\bar{y}_1 = 1$. Show that decreasing ρ will advantage to increase the pulse width.

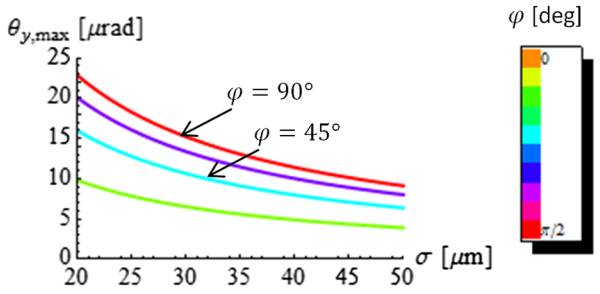

FIG. 6. The maximum kick angle $\theta_{y,\max}$ as a function of the beam size $\sigma_x = \sigma_y = \sigma_z$ for different crossing angle φ.

C. Maximum kick value $\theta_{y,\max}$

According to the previous discussion, if we design the distance between the low energy bunch's beam line and the storage ring beam line $d = \sqrt{2}\sigma_y$ and when the two bunches' centers arrive at $x_r = 0, z_r = 0$ with only a vertical separation d that means we have $\bar{y}_1 = 1, \bar{u}_1 = 0$, then the vertical kick reaches maximum $\theta_{y,\max} = \theta_y(x_r = 0, y_r = 0, z_r = 0) = \theta_{y0} f(\rho, \bar{u}_1 = 0, \bar{y}_1 = 1)$. The maximum kick angle $\theta_{y,\max}$ is still a function of the low energy bunch's 3-D beam size $\sigma_x, \sigma_y, \sigma_z$ and the crossing angle φ. In this section, we will discuss the dependence of $\theta_{y,\max}$ on $\sigma_x, \sigma_y, \sigma_z$ and φ, and find out the relative importance of $\sigma_x, \sigma_y, \sigma_z$ at different crossing angle. Based on the practical performance of the low energy linac compressor, the 3-D beam size $\sigma_x, \sigma_y, \sigma_z$ discussed are from 25 μm to 45 μm. The crossing angle discussed is from 0° to 90°.

We plot the maximum kick $\theta_{y,\max}$ as a function of the crossing angle φ for the low energy beam size $\sigma_x = \sigma_y = \sigma_z$ in Fig. 5. The kick angle increases with the increase of the crossing angle when $\varphi > 5°$. And the plot also shows that the smaller the low energy beam size is, the stronger the kick is. In order to make the relation between the low energy beam size and the slice kick angle more clear, we also plot the dependence of the maximum kick angle on the beam size for different crossing angles in Fig. 6.

In general, we need large kick angle, then we need small 3-D beam size $\sigma_x, \sigma_y, \sigma_z$ and large crossing angle φ. If we consider the relative importance of the 3-D beam size to the kick value, we will notice that in Eq. (15) the vertical beam size σ_y of the low energy bunch and its other two beam size σ_x, σ_z locate at different positions in the scaling parameter ρ, and in the nominal kick function Eq. (16) only the vertical beam size σ_y appears. In addition, we remark that the crossing angle φ influences the relative importance of σ_x and σ_z to the scaling parameter ρ.

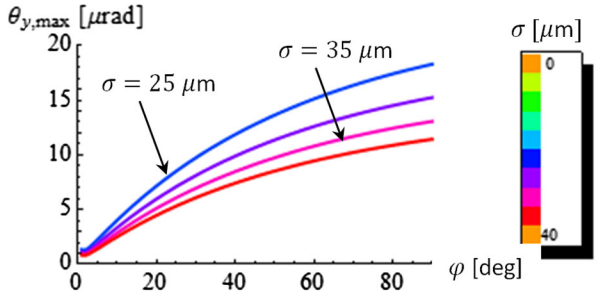

FIG. 5. The maximum kick angle $\theta_{y,\max}$ as a function of the crossing angle φ for different beam size σ when $\sigma = \sigma_x = \sigma_y = \sigma_z$.

With the vertical beam size σ_y fixed, we found in the range of crossing angle 0°–90°, to obtain the same kick angle smaller σ_x is more efficient than smaller σ_z. To see this, we choose $\sigma_y = 35$ μm as an example, and then we plot several contour figures of the kick value as a function of the longitudinal and horizontal beam size σ_x, σ_z for different crossing angle $\varphi = 22.5°, 45°, 67.5°, 90°$ in Fig. 7. The color represents the values of the kick angle. The more it is close to the yellow, the larger the kick angle is. The same black dash lines present the same kick values and the slope of the dash line indicates which beam size influences the kick angle more. The steeper the slope is, the less important σ_x is while the more important σ_z is to the kick. For example, the top-right plot ($\varphi = 45°$) in Fig. 7 shows that to obtain the same kick angle it is more efficient to short the low energy bunch's longitudinal beam size σ_x than to short its horizontal beam size σ_z. While the bottom-right plot ($\varphi = 90°$) in Fig. 7 indicates that the longitudinal beam size σ_x and the horizontal beam size σ_z have the same importance to kick angle when the crossing angle is $\varphi = 90°$.

The relative importance between the vertical beam size σ_y and the other two beam size σ_x, σ_z is complicated. Therefore we limit our discussion in the practical range of 25 μm–45 μm for the 3-D beam size. To figure out the relative importance of σ_x and σ_y we do the following scanning: (i) First we fix the value of σ_z and plot the contour plots of the kick angle as a function of σ_x and σ_y for different crossing angle $\varphi = 22.5°, 45°, 67.5°, 90°$ with σ_y. (ii) Then we scan σ_z from 25 μm to 45 μm with the step size 1 μm to plot the corresponding contour figures as step 1. Comparing these contour plots, we find that with the increase of the crossing angle the slope of the contour line will rotate clockwise. That means the importance of σ_y to the kick value is gradually increasing while the importance of σ_x is decreasing with the increase of the crossing angle.

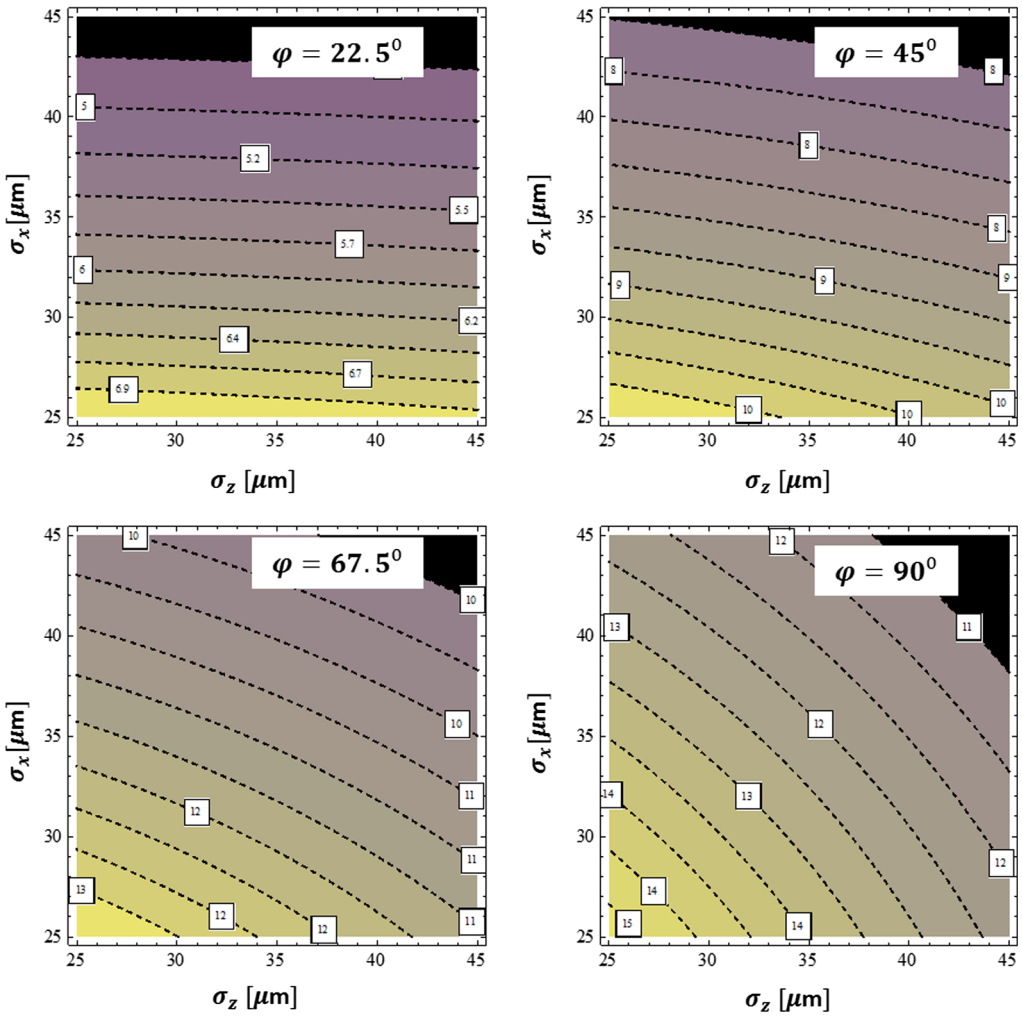

FIG. 7. Kick angle contour for $\sigma_y = 35$ μm. These pictures show the contour of the maximum kick angle $\theta_{y,\max}$ as a function of the longitudinal and horizontal beam size σ_x, σ_z for different crossing angle $\varphi = 22.5°, 45°, 67.5°, 90°$. The color represents the values of the kick angle. The more it is closer to the yellow, the larger the kick angle is.

We also find the influence of the horizontal beam size σ_z on the rotation and the relative slope value can be ignored in the discussed range of 25 μm–45 μm for the 3-D beam size. As an example for $\sigma_z = 35$ μm, the contour plots of the kick value as a function of the longitudinal and vertical beam size σ_x, σ_y for different crossing angle are shown in Fig. 8. The clockwise rotation of the contour line clearly indicates that to reach a kick value, for 45° crossing angle smaller σ_x is more important than smaller σ_y as shown in the top-left plot of Fig. 8, while for 90° crossing angle to short σ_y is more efficient than do σ_x as shown in the bottom-left of Fig. 8. We do the same scanning process to study the relative importance of σ_y and σ_z. The results, which are independent from the value of σ_x in the discussed range of 25 μm–45 μm for the 3-D beam size, show that a smaller vertical beam size σ_y is more important to the kick value than a smaller horizontal beam size σ_z for the crossing angle discussed. An example plot is shown in Fig. 9.

Table I gives a conclusion about the relative importance of the 3-D beam size to the kick value $\theta_{y,\max}$ for different crossing angle situations, i.e., for 45° crossing angle, to increase the kick angle shortening the longitudinal beam size σ_x is the most efficient way and for 90° crossing angle shortening the vertical beam size σ_y is more efficient than shortening σ_x and σ_z. These conclusions are justified in the range discussed around 25 μm–45 μm of 3-D beam size. The characteristics of the low energy bunch's 3-D beam size with different weights on the kick value makes the optimization of the low energy beam size more flexible. For some examples in Table II, if we manipulate relative beam size in different directions we can obtain different kick values.

D. Slice width

The width of the slice beam is another important parameter. From the expression of $\bar{u}_1$ in Eq. (15), we have

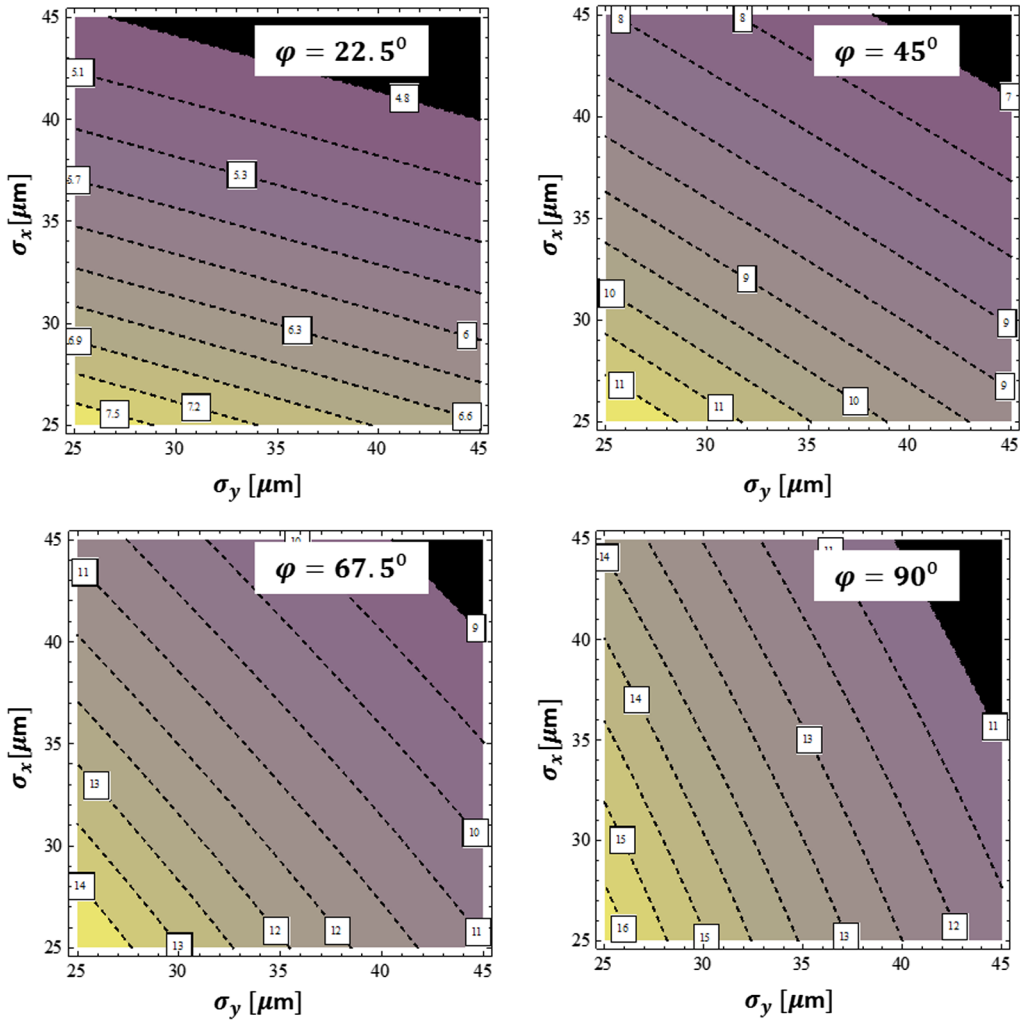

FIG. 8. Kick angle contour for $\sigma_z = 35$ μm. These pictures show the contour of the maximum kick angle $\theta_{y,\max}$ as a function of the longitudinal and vertical beam size σ_x, σ_y for different crossing angle $\varphi = 22.5°, 45°, 67.5°, 90°$. The color represents the values of the kick angle. The more it is closer to the yellow, the larger the kick angle is.

$$z_r = \bar{u}_1 \sqrt{2\sigma_x^2 + 2\sigma_z^2 \left(\frac{1-\cos\varphi}{\sin\varphi}\right)^2} + \left(\frac{\cos\varphi - 1}{\sin\varphi}\right) x_r. \tag{17}$$

This equation shows the slice width is affected by two independent terms: one term, being proportional to $\bar{u}_1$, due to the vertical kick from the linac bunch and the other term, being proportional to x_r, due to the horizontal crossing time of the low energy bunch when it passes across the high energy bunch from top. These terms add in quadrature to provide the slice width. To estimate the slice width, we assume the horizontal distribution of the storage ring bunch is Gaussian, and we also approximate the profile of $\bar{u}_1$ as Gaussian. Equation (17) shows the crossing angle φ influences the vertical kick term $\bar{u}_1$ and the horizontal crossing time term x_r. It is possible to reduce the pulse length due to the crossing time by reducing the crossing angle, for example from 90° to 45° between the forward direction of the linac beam and the storage ring beam. This is illustrated in Fig. 10 showing for 45° crossing angle the linac bunch has a velocity component parallel to the storage ring bunch making the slice shorter. We display this effect using the contour plots in Fig. 11 which shows the phase space distribution with color scale representing the kick angle for the 90° crossing and 45° crossing, respectively. The parameters used to plot Fig. 11 are the same as the example in Sec. III A. Using the same way in Sec. III A, the estimated RMS value of bunch length decreases from 190 fs for 90° crossing angle to 107 fs for 45° crossing angle at the expense of a reduction of the maximum vertical kick angle $\theta_{y,\max}$ from 13 μrad to 9 μrad. More numerical examples are given in Table II. In Fig. 12 we plot an example curve about the variation of the estimated RMS slice width with the crossing angle. When the 3-D beam size of the low energy bunch keep the same value, the slice width is independent of the charge of the low energy bunch. Therefore the decrease of the kick angle because we choose

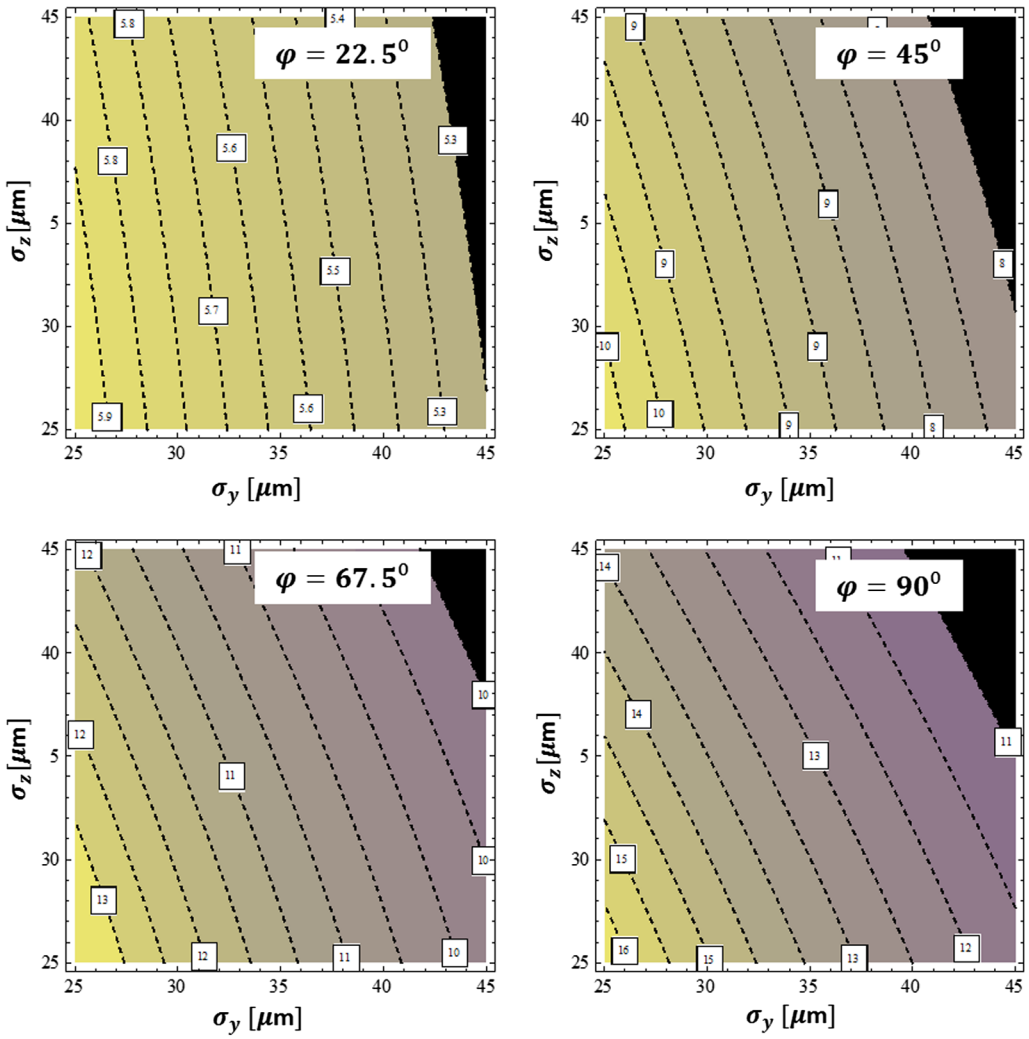

FIG. 9. Kick angle contour for $\sigma_x = 35$ μm. These pictures show the contour of the maximum kick angle $\theta_{y,\max}$ as a function of the vertical and horizontal beam size σ_y, σ_z for different crossing angle $\varphi = 22.5°, 45°, 67.5°, 90°$. The color represents the values of the kick angle. The more it is closer to the yellow, the larger the kick angle is.

a smaller crossing angle to shorten the slice width can be made up by increasing the charge of low energy bunch. At the same time, due to the space charge effects, with increasing the charge of low energy bunch we also need to increase the energy of low energy bunch to keep the same 3-D beam size.

TABLE I. The relative importance of the 3-D beam size $\sigma_x, \sigma_y, \sigma_z$ to the kick angle for different crossing angle, i.e., $\sigma_y < \sigma_x = \sigma_z$ means that to reach a kick value smaller vertical beam size σ_y is more important and the longitudinal and horizontal beam size σ_x, σ_z has the same weight on the kick value.

crossing angle	relative importance
22.5°	$\sigma_x < \sigma_y < \sigma_z$
45°	$\sigma_x < \sigma_y < \sigma_z$
62.5°	$\sigma_y < \sigma_x < \sigma_z$
90°	$\sigma_y < \sigma_x = \sigma_z$

IV. HORIZONTAL KICK θ_{xr} AND LONGITUDINAL ENERGY MODULATION $\Delta\gamma$

When the low energy linac bunch crossing pass through the high energy storage ring bunch, except the vertical kick θ_y the storage ring bunch also experiences the horizontal kick θ_{xr} and the longitudinal energy modulation $\Delta\gamma$ induced by the low energy bunch's electromagnetic field.

A. Horizontal kick θ_{xr}

According to Eq. (4), the horizontal kick force on storage ring electron is expressed as

$$F_{xr} = \frac{eq_2}{4\pi\varepsilon_0}\frac{\gamma_2}{S^3}[(x_1 - x_2)\sin\varphi + (z_1 - z_2)(\beta_1\beta_2 - \cos\varphi) + ct(\beta_1\beta_2 - 1)\sin\varphi]. \quad (18)$$

TABLE II. Kick parameters for different crossing angle and different low energy beam size for the example situation in Sec. III A.

Case	φ [°]	σ_x [μm]	σ_y [μm]	σ_z [μm]	$\theta_{y,\max}$ [μrad]	$\theta_{x,\max}$ [μrad]	τ_{RMS} [fs]	$\Delta\varepsilon_{y,\mathrm{kick}}$ [$\%\varepsilon_y$]	$\Delta\varepsilon_{x,\mathrm{kick}}$ [$\%\varepsilon_x$]
1	45	30	35	35	9.92	8.7	100	51.2	0.4
2	45	35	30	35	9.60	8.1	105	50.5	0.4
3	45	35	35	30	9.25	8.0	106	47.6	0.4
4	45	35	35	35	9.00	7.9	107	45.7	0.4
5	90	35	30	35	14.0	13.0	185	183	1.0
6	90	30	35	35	13.5	12.9	185	169	1.0
7	90	30	35	30	14.0	13.6	179	177	1.0
8	90	35	35	35	13.0	12.3	190	163	1.0

Following the similar process of deriving the vertical kick θ_y, we have the horizontal kick function as follows:

$$\theta_{xr} = -\frac{eq_2Z_0c}{2\pi E_1}\times\frac{(1-\cos\varphi)[1+\gamma_2^2\beta_1\beta_2+(1-\gamma_2^2)\cos\varphi]}{\gamma_2\sqrt{\gamma_2^2(1-\cos\varphi)^2+\sin^2\varphi}} \times\frac{1}{\sqrt{2[\sigma_x^2\sin^2\varphi+\sigma_z^2(1-\cos\varphi)^2]}}\times f_x(\rho,\bar{u}_1,\bar{y}_1) \tag{19}$$

with the profile function

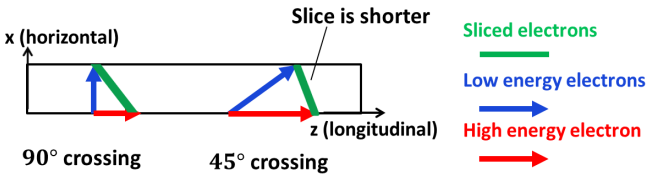

FIG. 10. Illustration of using 45° crossing to reduce crossing time and reduce the slice pulse length.

$$f_x(\rho,\bar{u}_1,\bar{y}_1) = \int_0^\infty \mathrm{Re}[W(-\bar{y}_1+iu)] \times[e^{-(\frac{u}{\rho}+\bar{u}_1)^2}-e^{-(\frac{u}{\rho}-\bar{u}_1)^2}]du \tag{20}$$

and the same scaling parameters $\rho,\bar{u}_1,\bar{y}_1$ as θ_y in Eq. (15). Notice that the horizontal profile function f_x is different from the vertical profile function f_y in Eq. (14). The plot of the profile function f_x in Fig. 13 shows the maximum and minimum kick value located at $\bar{y}_1=0,\bar{u}_1=-1$ and $\bar{y}_1=0,\bar{u}_1=1$, respectively. We also plot the profile f_x as a function of $\bar{u}_1$ on axis $\bar{y}_1=0$ in Fig. 14 and as a function of $\bar{y}_1$ on axis $\bar{u}_1=-1$ in Fig. 15. Figure 14 and Fig. 15 are different from the vertical kick's plots Fig. 4 and Fig. 3 in their dependence with the scaling parameter ρ. With the increase of ρ, f_x increases, while f_y decreases. The increase of the angular divergence increases the emittance of the storage ring bunch and then sets limitation on the system's repetition rate [13]. For the parameters in the example in Sec. III A, the maximum of the horizontal kick angle is

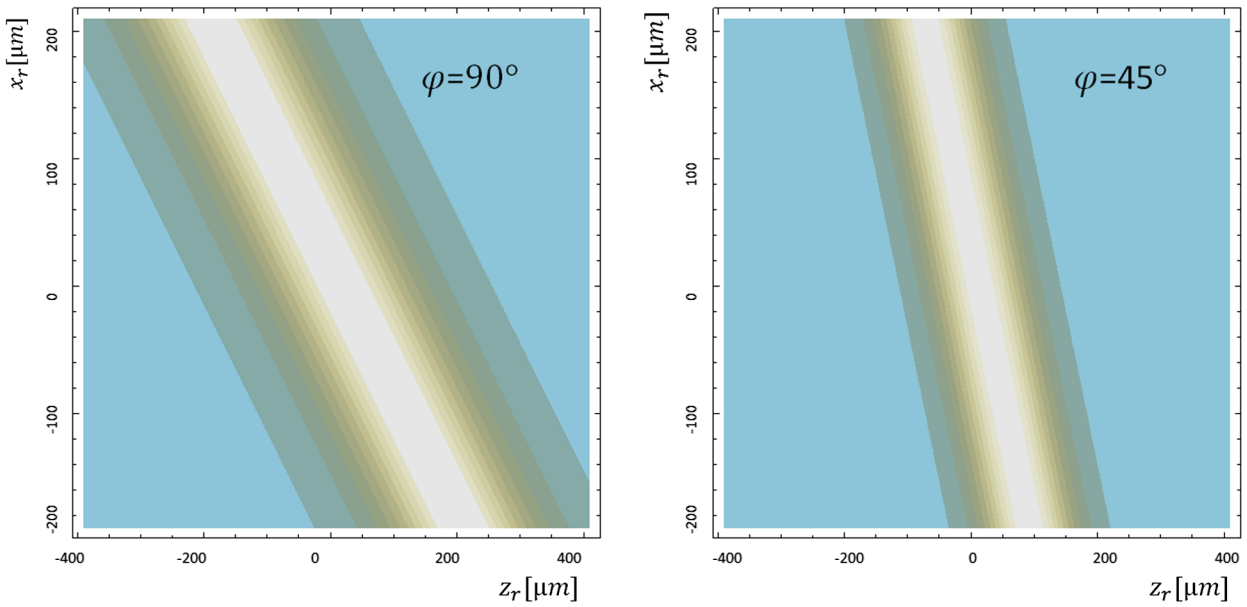

FIG. 11. Contour plots of the kick angle in xz phase space cutting at $y=0$ for different crossing angle $\varphi=90°$, $\varphi=45°$. Show the reduction of the crossing angle can reduce the slice width induced by the crossing time.

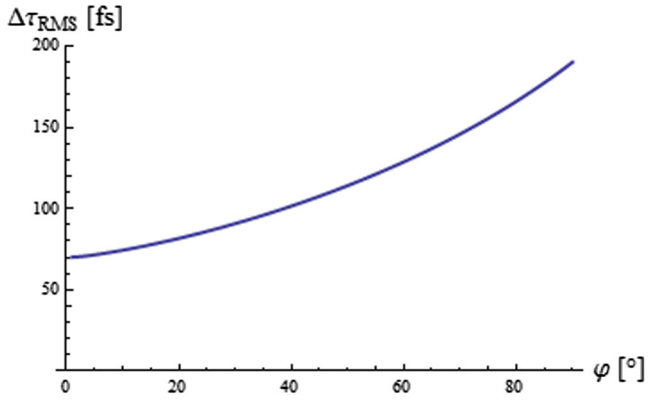

FIG. 12. Estimated slice bunch width τ_{RMS} is reduced with the decrease of the crossing angle φ.

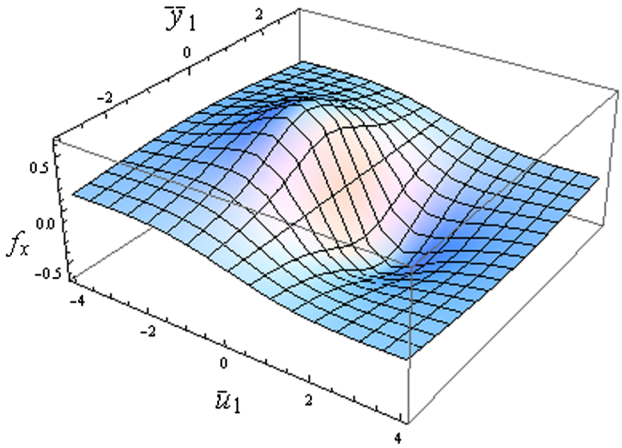

FIG. 13. Profile function f_x.

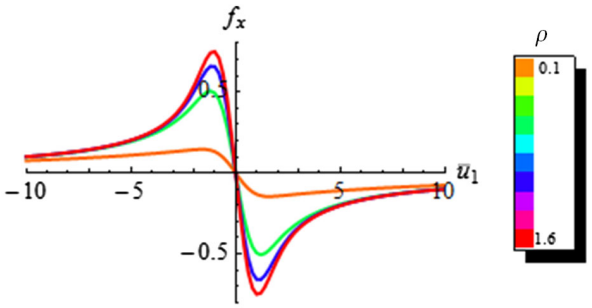

FIG. 14. Profile on axis $\bar{y}_1 = 0$. The maximum f_x locates at $\bar{u}_1 = -1$. Large ρ corresponds to large f_x.

12 μrad for 90° crossing and 7.9 μrad for 45° crossing. The estimated horizontal emittance increase due to the horizontal divergence increase is $1\%\epsilon_x$ for 90° and $0.4\%\epsilon_x$ for 45°, respectively. The horizontal emittance increase is much smaller than the vertical emittance increase due to the vertical divergence increase which is $163\%\epsilon_y$ for 90° and $45.7\%\epsilon_y$ for 45°, respectively. More numerical examples are given in Table II. Therefore the repetition rate

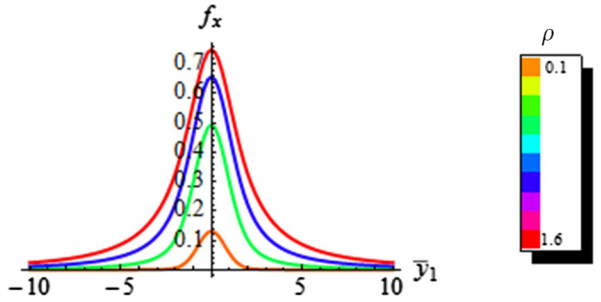

FIG. 15. Profile on axis $\bar{u}_1 = -1$. Large ρ corresponds to large f_x.

of the e-beam slicing system is limited by the vertical emittance increase and the horizontal angular divergence increase can be ignored.

B. Longitudinal energy modulation $\Delta\gamma$

According to Eq. (4), the longitudinal force exerting on the storage ring bunch by the low energy bunch can be expressed as

$$F_{zr} = \frac{eq_2}{4\pi\epsilon_0}\frac{\gamma_2}{S^3} \times [(x_1 - x_2)\cos\varphi + (z_1 - z_2)\sin\varphi + ct(1 - \cos\varphi)]. \quad (21)$$

The energy change induced by the longitudinal force F_{zr} is

$$d\gamma_1 = \frac{F_{zr}}{mc^2}dz_r = \frac{F_{zr}}{mc}dt. \quad (22)$$

We integrate $d\gamma_1$ over the crossing time to obtain the energy modulation $\Delta\gamma_{\text{point charge}}$ induced by a point charge in the low energy bunch 2. Then we integrate $\Delta\gamma_{\text{point charge}}$ over the whole low energy bunch 2. Finally, we obtain the slice energy modulation induced by the low energy bunch's longitudinal force exerted on the storage ring bunch as follows:

$$\Delta\gamma = -\frac{eq_2Z_0c}{2\pi mc^2} \times \frac{[\gamma_2^2(1-\cos\varphi)+\cos\varphi]\sin\varphi}{\gamma_2\sqrt{\gamma_2^2(1-\cos\varphi)^2+\sin^2\varphi}} \times \frac{1}{\sqrt{2[\sigma_x^2\sin^2\varphi + \sigma_z^2(1-\cos\varphi)^2]}} \times f_x(\rho, \bar{u}_1, \bar{y}_1) \quad (23)$$

where $f_x(\rho, \bar{u}_1, \bar{y}_1)$ is given by Eq. (20). For the beam parameters in the example in Sec. III A, the maximum energy modulation is $\Delta\gamma = 0.072$ at 90° crossing and $\Delta\gamma = 0.11$ at 45° crossing. Therefore compared with $\gamma = 6000(3\ \text{GeV})$, the energy modulation induced by the Coulomb force can be ignored.

V. REACTION OF STORAGE RING BUNCH TO LINAC BUNCH

To calculate the reaction of high energy bunch to low energy bunch, we use Eq. (13) and change notation. Now "2" refers to high energy bunch and "1" refers to low energy bunch. Then for the high energy bunch, the axis "+x," "+y" and "+z" are the longitudinal, vertical, and horizontal direction, respectively. Here, we use the beam parameters in Sec. III A as an example to explain that the reaction can be ignored.

At the kick point, the relevant parameters of the high energy bunch are $\sigma_x = 15\ \text{ps} \times 3 \times 10^8\ \text{m/s} = 4.5\ \text{mm}$, $\sigma_y = \sqrt{25\ \text{m} \times 10^{-11}\ \text{m}} = 15.8\,\mu\text{m}$, $\sigma_z = \sqrt{3.8\ \text{m} \times 10^{-9}\ \text{m}} = 61.6\,\mu\text{m}$, $q_2 = \frac{0.5\ \text{A} \times 2.63\ \mu\text{s}}{1000} = 1.3\ \text{nC}$ (For beam current of 0.5 A, assume 1000 bunches, with the revolution time of 2.63 μs, we have the bunch charge as 1.3 nC), $E_1 = 20\ \text{MeV}$, $\gamma_2 = \frac{3\text{GeV}}{0.511\text{MeV}} = 6000$. In order to estimate the maximum reaction, we choose crossing angle $\varphi = 90^\circ$, then $\theta_y(90^\circ) = \frac{eq_2 Z_0 c}{2\pi E_1} \frac{\gamma_2}{\sqrt{\gamma_2^2+1}} \frac{1}{\sqrt{2}\sigma_y} \times f_y(\rho, \bar{u}_1, \bar{y}_1) = 0.05 \times f_y(\rho, \bar{u}_1, \bar{y}_1)$, where $f_y(\rho, \bar{u}_1, \bar{y}_1)$ is the profile function. For this storage ring bunch, the profile parameter $\rho = \sqrt{\frac{\gamma_2^2}{\gamma_2^2+1} \cdot \frac{\sigma_x^2+\sigma_z^2}{\sigma_y^2}} = 285$. We choose the same situation as Sec. III A, then $\bar{u}_1 = 0, \bar{y}_1 = 1$. When $\rho \gg 1$, the profile function Eq. (14) becomes

$$
\begin{aligned}
&f_y(\rho \gg 1, 0, \bar{y}_1 = 1) \\
&= \int_0^\infty \text{Re}[W(iy)][e^{-(\rho y - \bar{y}_1)^2} - e^{-(\rho y + \bar{y}_1)^2}]dy \\
&= \frac{1}{\rho}\int_0^\infty \text{Re}\left[W\left(i\frac{y}{\rho}\right)\right][e^{-(y-\bar{y}_1)^2} - e^{-(y+\bar{y}_1)^2}]dy. \qquad (24)
\end{aligned}
$$

Due to $\bar{y}_1 = 1$, the contribution of the factor $[e^{-(y-\bar{y}_1)^2} - e^{-(y+\bar{y}_1)^2}]$ to the profile function f_y comes from $y \sim 1$, then we have $y/\rho \ll 1$. This leads to $W(i\frac{y}{\rho}) = 1$. Then we have

$$
\begin{aligned}
f_y(\rho \gg 1, 0, \bar{y}_1 = 1) &\approx \frac{1}{\rho}\int_0^\infty \left[e^{-(y-\bar{y}_1)^2} - e^{-(y+\bar{y}_1)^2}\right]dy \\
&= \frac{\sqrt{\pi}}{\rho}\text{erf}(\bar{y}_1), \qquad (25)
\end{aligned}
$$

where $\text{erf}(z) = \frac{2}{\sqrt{\pi}}\int_0^z e^{-t^2}dt$. Therefore, the profile function $f_y(\rho = 285, \bar{u}_1 = 0, \bar{y}_1 = 1) \approx 0.0052$ and the reaction angle on the linac bunch from the storage ring bunch is $\theta_y(90^\circ) = 0.087 \times f_y(\rho = 285, \bar{u}_1 = 0, \bar{y}_1 = 1) \approx 0.26\ [\mu\text{rad}]$. We assume the longitudinal beam size of the linac bunch is 35 μm. Then during the interaction time, the linac bunch's position will be changed about 0.016 μm in vertical direction which can be ignored when compared with the vertical beam size 35 μm.

VI. CONCLUSIONS

We presented formulas in Eq. (13), Eq. (19), and Eq. (23), which can be used to study the characteristics of the electron beam slicing. The slice bunch's profile is described by the profile function f_y, f_x. The maximum kick angle and the slice width can be manipulated through the low energy beam size σ_x, σ_y, σ_z and the crossing angle φ. With the variance of the crossing angle φ, the relative importance of the low energy beam size σ_x, σ_y, σ_z will be varied. Decreasing the crossing angle φ can significantly shorten the slice width at the expense of lowering the maximum kick angle $\theta_{y,\text{max}}$. Because the slice width is independent of the charge of the low energy bunch, the decrease of $\theta_{y,\text{max}}$ induced by the reduction of φ can be compensated by increasing the charge and the energy of the low energy bunch while keeping the same 3-D beam size. The influence of the horizontal angular divergence increase of the slice can be ignored, because the limitation of the system's repetition rate is set by the vertical emittance increase. The energy modulation of the slice induced by the kick is very small and can be also ignored. The reaction of the storage ring bunch on the low energy linac bunch can be ignored due to the small position change of the linac bunch included by the reaction. The formulas and the results present here are applied to the study of electron beam slicing in NSLS-II [13] and also are used to determine the target parameters of the low energy bunch to guide the design of the linac compressor [15].

ACKNOWLEDGMENTS

We would like to thank all colleagues of the accelerator group in NSLS-II BNL. This work was funded by DOE under Contracts No. LDRD12-023 and LDRD14-022.

[1] S. Ozaki, J. Bengtsson, S. Kramer, S. Krinsky, and V. Litvinenko, in *Proceedings of the 22nd Particle Accelerator Conference, PAC-2007, Albuquerque, NM* (IEEE, New York, 2007), p. 77.

[2] A. Zholents and M. Zolotorev, Phys. Rev. Lett. **76**, 912 (1996).

[3] R. W. Schoenlain, S. Chattopadhyay, H. H. W. Chong, T. E. Glover, P. A. Heimann, C. V. Shank, A. A. Zholents, and M. S. Zolotorev, Science **287**, 2237 (2000).

[4] K. Holldack, T. Kachel, S. Khan, R. Mitzner, and T. Quast, Phys. Rev. ST Accel. Beams **8**, 040704 (2005)

[5] G. Ingold, A. Streun, B. Singh, R. Abela, P. Beaud, G. Knopp, L. Rivkin, V. Schlott, Th. Schmidt *et al.*, in *Proceedings of the Particle Accelerator Conference, Chicago, IL, 2001* (IEEE, New York, 2001), p. 2656.

[6] C. Steier *et al.*, in *Proceedings of the 2003 Particle Accelerator Conference, Portland, OR* (IEEE, New York, 2003), p. 397.

[7] O. Chubar and P. Elleaume, in *Proceedings of the 6th European Particle Accelerator Conference, Stockholm, 1998* (IOP, London, 1998), p. 1177.
[8] A. Zholents, P. Heimann, M. Zolotorev, and J. Byrd, Nucl. Instrum. Methods Phys. Res., Sect. A **425**, 385 (1999).
[9] M. Katoh, Jpn. J. Appl. Phys. **38**, L547 (1999).
[10] M. Borland, Phys. Rev. ST Accel. Beams **8**, 074001 (2005).
[11] P. Emma, Nat. Photonics **4**, 641 (2010).
[12] F. Willeke and L. H. Yu, in *Proceedings of the 4th International Particle Accelerator Conference, IPAC-2013, Shanghai, China, 2013* (JACoW, Shanghai, China, 2013).
[13] A. He, F. Willeke, and L. H. Yu, Phys. Rev. ST Accel. Beams **17**, 040701 (2014).
[14] L. D. Landau and E. M. Lifshitz, *The Classical Theory of Fields* (Addison-Wesley Press, New York, 1951), p. 99.
[15] A. He *et al.*, in *Proceedings of the 4th International Particle Accelerator Conference, IPAC-2013, Shanghai, China, 2013* (JACoW, Shanghai, China, 2013).